

# Study of Solar Energetic Particles: their Source Regions, Flares and CMEs during Solar Cycles 23-24

\*Raj Kumar<sup>1</sup>, Ramesh Chandra<sup>1</sup>, Bimal Pande<sup>1</sup>, Seema Pande<sup>1</sup>

<sup>1</sup>Department of Physics, DSB Campus, Kumaun University, Nainital, India

## ABSTRACT

In this work, we examine the association between solar active regions and 152 solar flares, coronal mass ejections, and solar energetic particle (SEP) events over solar cycles 23–24 (1997–2017). The Coordinated Data Analysis Workshops (CDAW) center's GOES data in the energy channel  $> 10$  MeV (Major SEPs; solar proton events) with flux  $\geq 10$  pfu was used for our investigation. For the associated activities, we have analyzed the data from space born satellites namely: SOHO/LASCO and SDO/AIA. We found a moderate correlation (55%) between SXR flux and sunspot area i.e., active regions with larger sunspot areas generally generate larger flares. We found that most of the SEPs are originated from the magnetically complex active regions i.e., Hale class  $\beta\gamma\delta$  and  $\beta$ . Very few events were associated with unipolar active regions. Stronger GOES X-ray is linked to more impulsive events, as evidenced by the negative correlation (-0.40) between X-ray flux and SEP duration. In the active region  $\beta\gamma\delta$ , the highest average SEP intensity (2051 pfu) was detected. In the data set used, only 10% SEPs are found impulsive in nature, while the remaining 90% are gradual in nature. All the impulsive events had SEP intensity less than 100 pfu and most of the CMEs associated with these events were decelerated CMEs. We discovered that the majority of faster CMEs are linked to the most complex magnetic active regions. This indicates that high speed CMEs are produced by magnetically complex active regions. We discovered that 58 SEP events in our data set are linked to accelerated CMEs, while 82 are linked to decelerated CMEs. The highest average CME width is found corresponding to magnetically most complex active regions  $\beta\delta$ ,  $\gamma\delta$ ,  $\alpha\gamma\delta$  and  $\beta\gamma\delta$ , which shows that large CMEs are the consequences of magnetically complex active regions.

**Keywords:** Solar energetic particle events — Solar active region— Coronal mass ejections — Gradual SEP events — Impulsive SEP events.

\*Corresponding Author

Email: [rajchanyal@gmail.com](mailto:rajchanyal@gmail.com)

## 1. Introduction

High-energy particles with energies ranging from a few thousand electron volts to giga electron volts are known as Solar Energetic Particle (SEP) events, whereas Solar Proton Events (SPEs) have energies ranging from a few million electron volts to giga electron volts. Forbush saw the first SEP event in 1946 [1], and it was eventually identified as ground level enhancements [2]. Much earlier than the earliest observable evidence of SEP events Carrington (1859) [3] was the first to report solar flares. Thus, until the 1970s, the SEP events were thought to be a result of solar flares. After the discovery of Coronal Mass Ejections (CMEs) in the 1970s, a different theory for how SEP events are produced emerged [4] i.e., CME shocks generation and they were categorized as either impulsive or gradual SEP events [5–13].

Generally SEP events of very short duration are impulsive SEP events while the SEPs of long duration are termed as gradual SEP events. Gradual events are long duration events ranging from 1 to 3 days, while impulsive events are short lived in nature with the SEP duration of less than one day ( $< 1\text{-}20$  h) [14]. Every year, approximately one thousand impulsive events are observed while a few tens of large events are observed per year. In impulsive SEP events, the associated X-ray flares are also impulsive in nature, typically lasting up to an hour, whereas in gradual SEP events, the flare duration exceeds one hour [15, 16]. These two types of events can be categorized on the basis of energetic particle composition and radio observations [11]. Impulsive events are  $^3\text{He}$  rich events which are accompanied by type-III radio bursts [17]. These electron-rich events exhibit  $^3\text{He}/^4\text{He}$  ratios, ranging from 1,000 to 10,000 and Fe/O ratios up to a factor of 10.

The gradual events are proton rich events which have Fe/O ratio up to 0.1. These events do not have a measurable amount of  $^3\text{He}/^4\text{He}$  ratios and are associated with type II radio bursts [13, 18]. The gradual events are observed from both the east and west longitudinal distribution of flares, while the impulsive events are mostly observed from western longitudinal flare sites [13, 14].

According to Gopalswamy *et al.*, 2007 [19], SEPs can be the consequences of energetic CMEs. Generally, gradual SEP events are considered to be originated due to CME driven shocks while impulsive SEP events are originated due to the solar flares associated with magnetic reconnection [13, 14, 20- 23].

Strong SEPs are associated with the stronger shocks which are originated from high speed CMEs [24-26] with average speed of  $\approx 1500 \text{ km s}^{-1}$  [27] and  $\approx 1240 \text{ km s}^{-1}$  [28]. Many authors looked for a desired strong correlation between the parameters of CME on one hand and SEPs on another, but didn't find a strong correlation between these parameters [29-33]. According to Gopalswamy *et al.*, 2009 [34], CME–CME interaction, CMEs deflection from the coronal hole regions etc. might be the reasons for the occurrence of this weak correlation.

Another possible mechanism of the impulsive SEPs is flare reconnection process [35, 36]. Numerous statistical studies have shown that the correlation between SEPs parameters and solar X-ray flux is found weak [37, 38]. In a recent study, Kumar, *et al.*, 2020 [28] found a weak correlation ( $r = 0.40$ ) between SEP intensity and X-ray flux. So it is considered that neither the CME shocks nor the flare reconnection processes are separately responsible for the generation of SEP events, but both the mechanisms as a whole contribute for the same, although their relative contribution is not exactly clear [39, 40].

Magnetic topology of active regions (ARs) with the shock and reconnection mechanisms should also be taken into account for solving the puzzle of SEPs generation mechanism [28, 41-45]. Numerous studies have explored the relationship between active region complexity and the occurrence of solar flares and CMEs, revealing that greater magnetic field complexity increases the likelihood of generating intense flares and large CMEs [46, 47]. The large active regions having more complex magnetic structures and sufficient stored magnetic energy are responsible for the generation of strong flares and CMEs [42, 48-50].

We therefore present here a study of SEPs, impulsive and gradual SEP events with their linked source regions, associated CMEs and soft X-ray flares. The relative contribution of CMEs, solar flares and magnetic complexity of source regions to the occurrence of SEPs is described with their correlation study. Distribution of SEP intensity, X-ray flux, CME speed, CME acceleration and deceleration is examined with different type of magnetically complex (Hale classes) active regions. Section 2 contains the description of observations. In section 3, results and discussion are described, while section 4 presents the Conclusions.

## 2. Observations

For this study we have taken 152 SEPs, which are associated with CMEs and solar flares. These SEPs are taken in the energy channel  $>10 \text{ MeV}$  during solar cycle 23 and 24 from 1997 to 2017. 106 SEPs are reported during solar cycle 23 and during cycle 24, 46 SEPs are reported in

this energy channel. The SEP intensity is given in the unit of particle flux unit (pfu) and  $1 \text{ pfu} = 1 \text{ proton cm}^{-2}\text{s}^{-1}\text{sr}^{-1}$ . The SEP list is downloaded from Coordinated Data Analysis Workshops (CDAW) data center ([https://cdaw.gsfc.nasa.gov/CME\\_list/sepe/](https://cdaw.gsfc.nasa.gov/CME_list/sepe/)) [34, 51]. Then each and every event is cross checked with the help of CME data taken from the Large Angle and Spectrometric Coronagraph (LASCO) [52] onboard Solar and Heliospheric Observatory (SOHO) satellite.

Association of each SEP event with CMEs and X-ray flares is cross verified with the help of the movies given in the LASCO Catalogue for each CME event (e.g., [https://cdaw.gsfc.nasa.gov/movie/make\\_javamovie.php?date=19971104&img1=lasc2rdf](https://cdaw.gsfc.nasa.gov/movie/make_javamovie.php?date=19971104&img1=lasc2rdf)). GOES X-ray data, which can be found at <https://satdat.ngdc.noaa.gov/sem/goes/data/plots/>, is used to cross-verify SEPs that are not included in the LASCO catalogue (CME events are absent for these durations).

The CME source location is taken again using images and movies available at SOHO/LASCO CME catalogue (soho/lascocme catalogue/java movies/). We have carefully checked the source location and active regions (ARs) from GOES soft X-ray flare data. Corresponding to the each active region we have taken the Hale class magnetic classification [53, 54] of the magnetic complexity from <https://www.swpc.noaa.gov/products/solar-region-summary> and [www.solarmonitor.org](http://www.solarmonitor.org). According to original Hale classification, designation ( $\alpha$ ) is for those ARs which have unipolar sunspot or sunspot group. If two sunspots or sunspot groups are of opposite polarities in a region, that active region is assigned as ( $\beta$ ). Hale class ( $\gamma$ ) is defined as the AR in which positive and negative polarities are distributed in a very complex way, these can't be separated from each other to classify them as a bipolar sunspot group. In 1965, Kunzel [62] proposed a new classification of ARs in addition to existing Hale classes, which was named as ( $\delta$ ) class of ARs. In this classification within a single penumbra separated by no more than  $2^\circ$  in heliographic distance (24 Mm or 33" at disk center), at least one sunspot contains opposite magnetic polarity [54]. Gradual and impulsive SEP events are extracted from the available list of SEPs. In the given list of major SEP event data the end time of the events is not available. Several researchers calculated SEP end times for their studies on SEP duration with some solar activity features [55-57]. But they didn't list the end times and subsequently the duration of SEPs. Firoj et al. 2022 [58] did a study on duration and fluence of major SEP events and listed the end times of SEPs but they had used only 34 major SEP events.

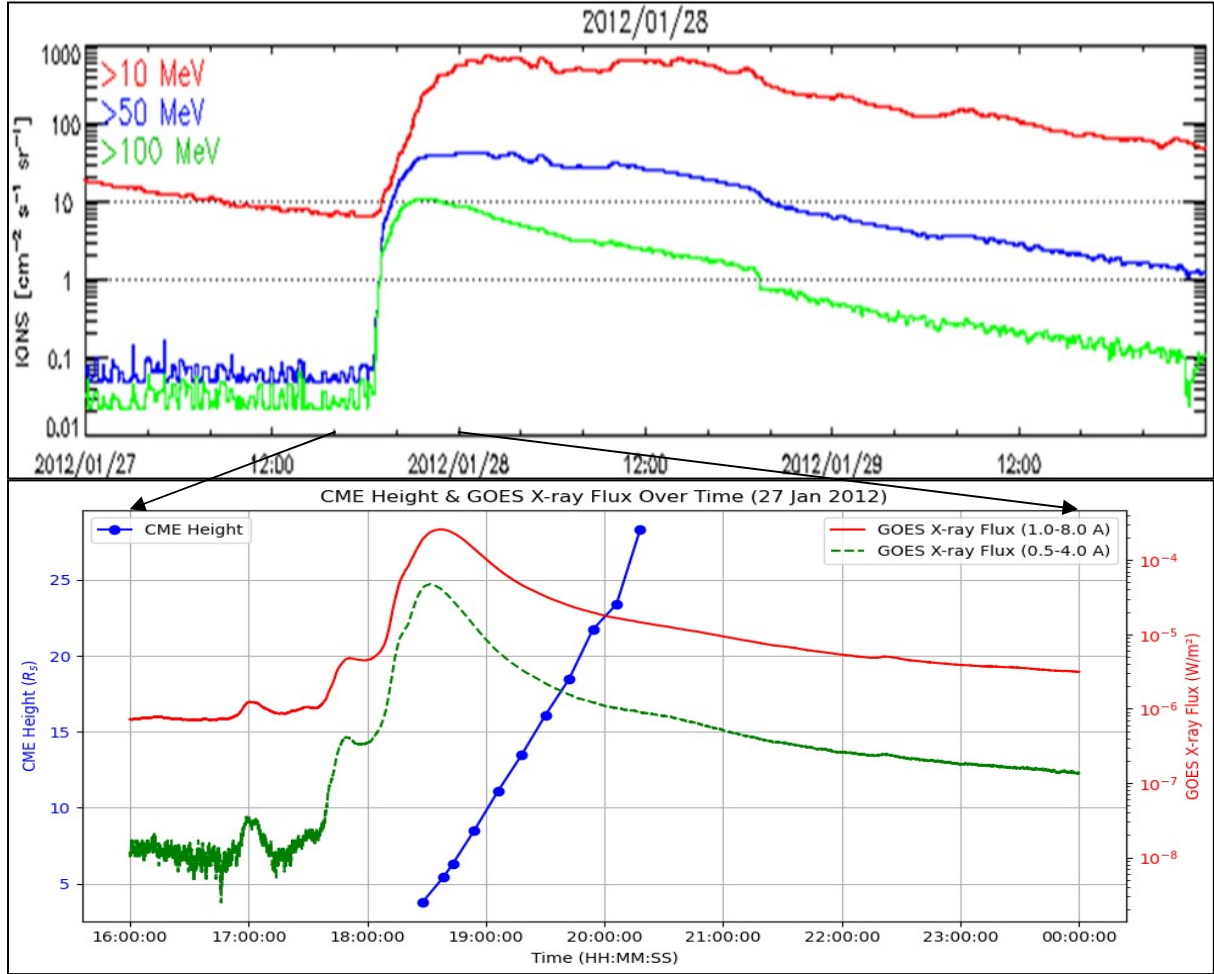


**Figure 1** *An example of gradual SEP event in the energy channel  $> 10$  MeV on 27 January, 2012 with associated CME and solar X-ray flare. Top panel: Temporal evolution of proton flux. Bottom panel: Corresponding GOES flare temporal evolution in 1-8 A (red colour) and 0.5-4 A (green colour) overlaid by associated CME (blue colour).*

We have calculated the SEP duration for 148 SEP events. Four events are corresponding to those events for which end time was not shown because of the unavailability of the CME data on subsequent days. We have determined the duration by noting the onset time of each event and end phase is considered at the time when the event is decaying to the equivalent background intensity level of onset time. Some of the events are overlapping events, for such events end time is the onset time of the next event and at the end of the last overlapped event, end phase is taken at the time when it reaches the background intensity level.

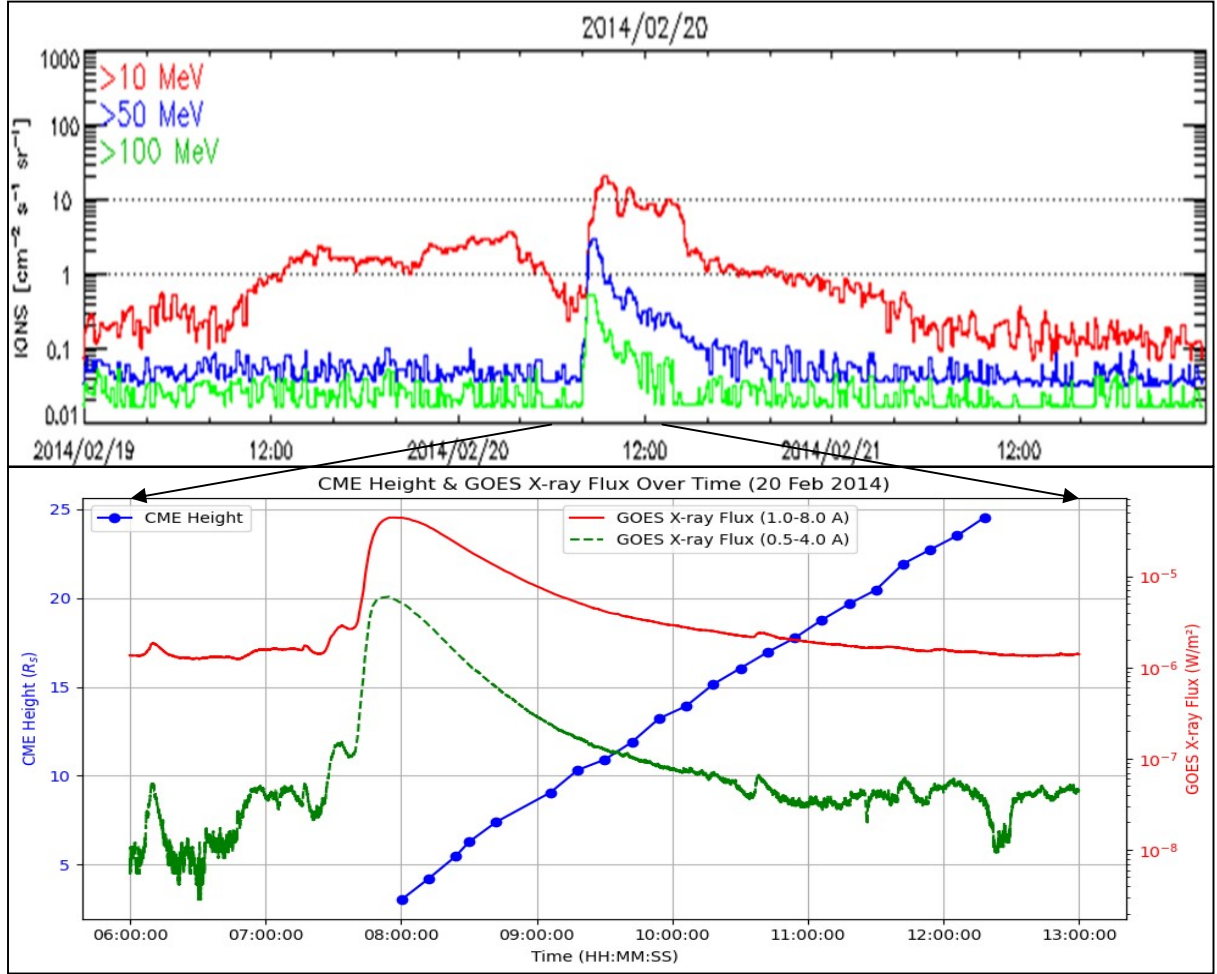


**Figure 2** *Example of impulsive SEP event of 20 February, 2014. Other information is same as described in figure 1.*

In Figure 1, an example of a gradual SEP event is presented, this event has the SEP duration of 4.58 days with the start time of 18:55 UTC on 27-01-2012 and end time of 8:52 UTC on 01-02-2012. This event was associated with a halo CME having a speed of  $2508 \text{ km s}^{-1}$  and accompanying X-ray is a X1.7 GOES class flare with the source region having  $\beta\gamma$  magnetic configuration. Figure 2 presents the example of an impulsive SEP event with the SEP duration of 0.8 days with the start time of 8:15 on 20-02-2014 and event was completed at 3:33 UTC of 21-02-2014. This SEP event is associated with a halo CME having speed of  $948 \text{ km s}^{-1}$  and related X-ray flare has a M3.0-class flare with the source region having complexity  $\alpha$ . The source



location of the mentioned SEP event is S15W73. The detailed list for the SEP duration of these events is provided here for the future use in Appendix as Table 2.

### 3. Results and Discussion

Different statistical results corresponding to the analysis of SEPs with different activity features like SEP duration, solar X-ray flares, CME properties and magnetic complexity of active regions are presented in following sections.

#### 3.1 Association of Flare Properties with SEPs and Hemispheric Distribution

We have calculated the duration of each SEP event and classified them in impulsive and gradual events according to the definition given in the introduction section. The duration of SEPs is plotted against SEP intensity in the Figure 3(a).

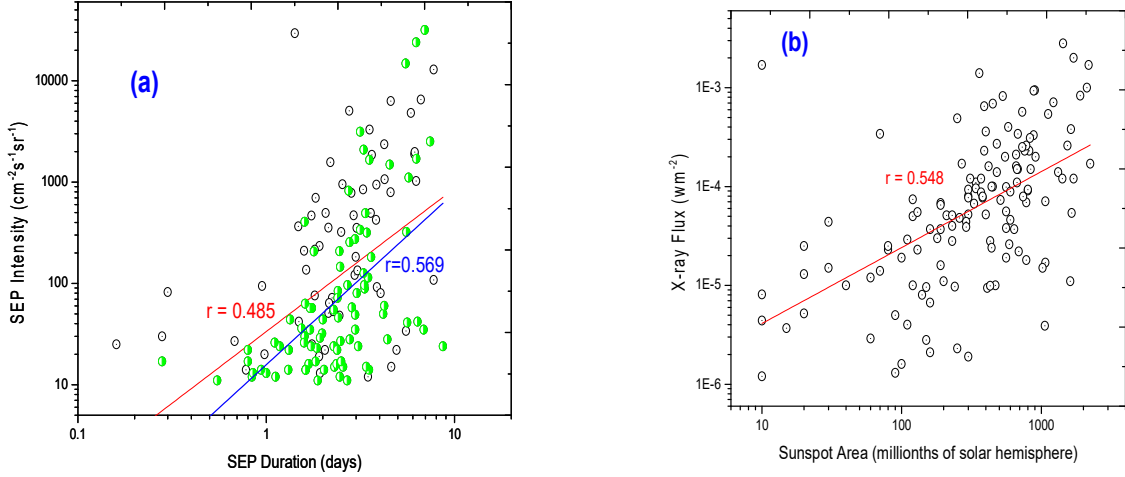


**Figure 3** Correlation study between SEP intensity and SEP duration (panel-a) taking all the events in to account (red colored line and black balls) and removing overlapping events (blue colored line and green balls) and between X-ray flux and Sunspot area (total sunspot area present in the active region) (panel-b).

For a scattered plot, the Pearson's correlation coefficient 'r' is a measure of how close the observations are to a line of best fit. The Pearson's correlation coefficient is given by

$$r = \frac{n \sum xy - \sum x \sum y}{\sqrt{[n \sum x^2 - (\sum x)^2][n \sum y^2 - (\sum y)^2]}} \quad (1)$$

Where, n is the total number of x or y variables. Interchanging the variables x and y between two related parameters don't affect the correlation coefficient.

The correlation between SEP intensity and SEP duration is 0.49 for all the events taken in to account. Further for the better association between these parameters, we have inspected all the events and found 35 overlapping SEPs. Now the correlation becomes stronger and the value is 0.57 (Figure 3(a)). In both the cases correlation is moderate; we can infer from this study that gradual nature of the SEPs is not only shown by increment in SEP intensity but by other parameters also like strong CME properties. Plotting the flare X-ray flux against sunspot area (*total sunspot area present in the active region*) (Figure 3(b)) yields a correlation coefficient of 0.55, suggesting a moderate correlation between the two. The X-ray flux is the flux measured in 1-8 Å wavelengths in the unit of  $\text{Wm}^{-2}$ . This full disk X-ray flux is measured by GOES satellite assuming sun as a star. It means active regions with larger sunspot areas generally generate larger flares. Larger will be the sunspot area more will be the magnetic flux so higher will be the probability of generating strong flares [42, 50]. However, the flare generation depends more on the magnetic complexity of the active regions [47, 59]. This study of magnetic complexity of ARs is described in section 3.2.

In Figure 4(a), we have plotted the distribution of SEP events in different hemispheres of the solar disk. We found that the latitudinal distribution varies between  $-40^\circ$  to  $+40^\circ$ , while longitudinal distribution spans the whole longitude range ( $-90^\circ$  to  $+90^\circ$ ). We found approximately equal distribution of SEP events in northern and southern hemispheres (71 in north and 68 in south). But we see a big difference in the distribution of events between eastern and western longitudes (31 in east and 114 in west), which is because of Parker's spiral lines [29, 30, 37]. Our analysis shows that although CME speeds and X-ray fluxes are higher in the eastern hemisphere, the average SEP intensity beyond  $40^\circ$  east is actually lower compared to that in the western hemisphere beyond  $40^\circ$  west.

80% of the events are located in the western hemisphere and only 20% are in the eastern hemisphere. In Figure 4(b), a time series of the latitudinal distribution is displayed for both the cycles. We found a trend of butterfly diagram for both the cycles i.e., migration of events from higher latitudes (here  $35^\circ$ ) towards equator ( $1^\circ$ ) and a shape of wings of butterfly is obtained. The SEP events are originated at the higher latitudes (both northern and southern hemispheres) at the beginning of the cycle and continuously shift towards the center of the disk as the cycle progresses.



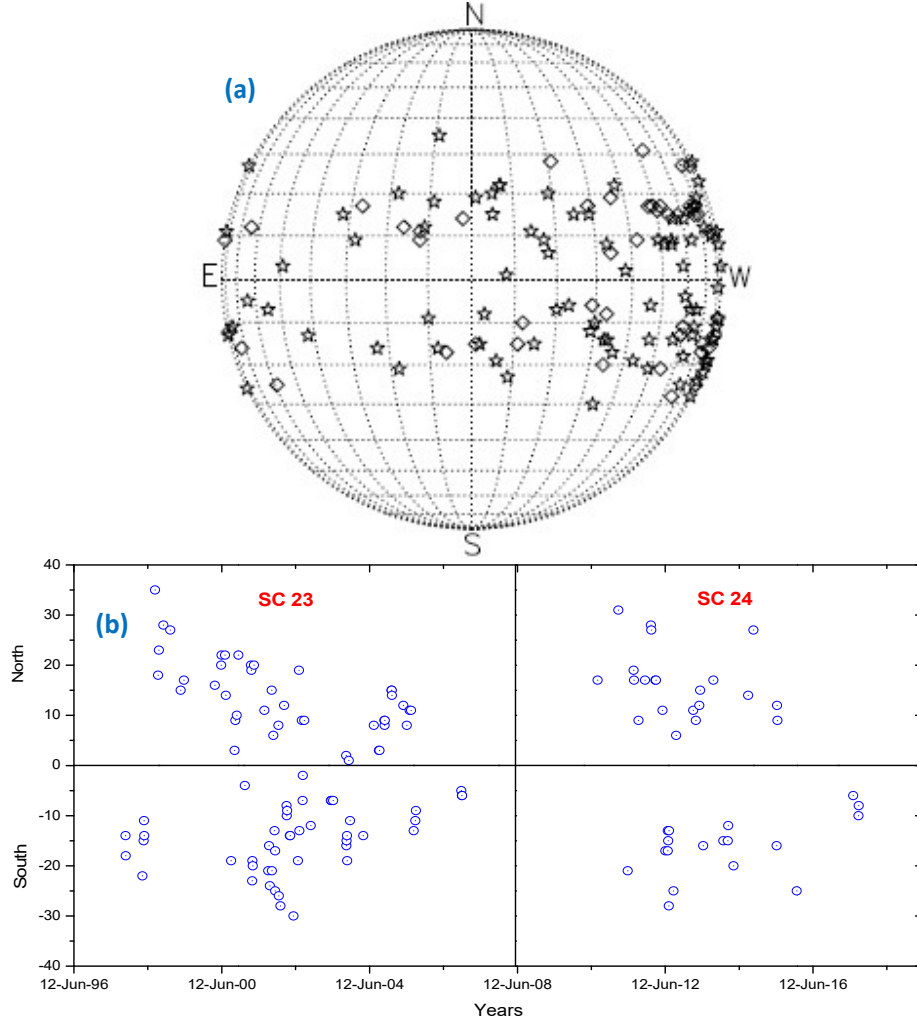


**Figure 4** *Source location of SEP events on solar disk (panel-a). Locations with asterisk (\*) are showing the events of cycle 23 and those with diamond (◇) showing the events of cycle 24. Latitudinal time series distribution of SEP events is shown in panel - b.*

A correlation analysis between SEP intensity and X-ray flux was conducted for solar cycles 23 and 24, which is presented in Figure 5 (a). We obtained a correlation coefficient of 0.46, indicating a moderate relationship between the two variables. Gopalswamy et al., 2003 and 2004 [30, 37] also reported a poor correlation of 0.41 between SEPs intensity and X-ray flare flux.

Our study of the correlation between SEP intensity and various X-ray flare classes (Figure 5 (b, c, d)) shows that the correlation strengthens as flare intensity increases, from weaker (C class) to stronger flares (X class). The correlation between C-class flares and SEP intensity is 0.06 only, while that between M-class and SEP intensity becomes 0.24. This

correlation increases to 0.37 when we consider X-class flares with SEP intensity. The negative correlation between flare C-class and SEPs intensity is 0.06 (close to zero), which shows no relation between them. The reason for obtaining moderate correlation between these two parameters can be because of the association of SEP events not only with solar flares but with other phenomena also like magnetic topology of active regions and shock wave generated CMEs.

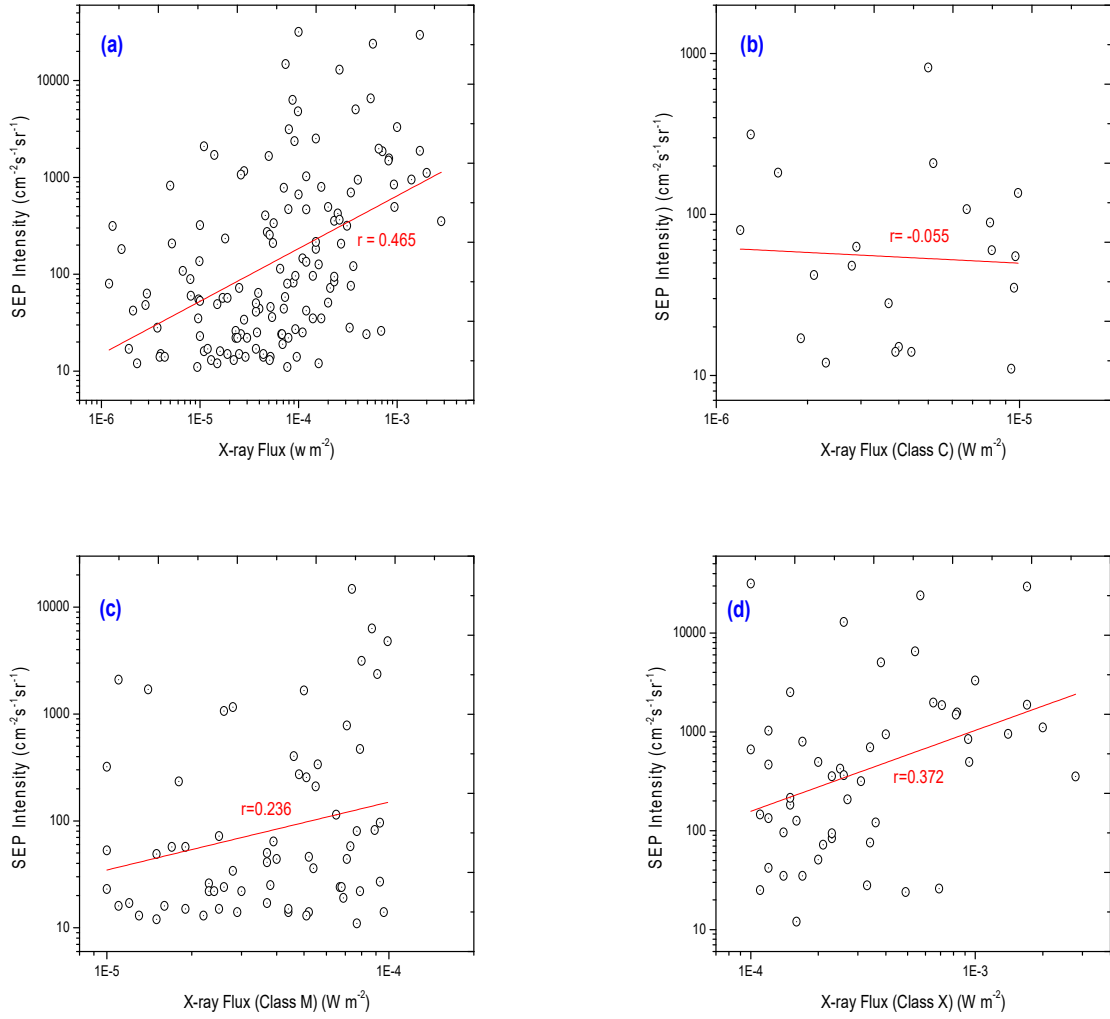


**Figure 5** Variation of total X-ray flux with SEP intensity and class wise variation of the same with SEP intensity.

In Figure 6, the SEP duration is plotted against X-ray flux. In Figure 6(a), all the events are considered. We found a weak correlation between X-ray flux and SEP duration which is just

0.26. But when we considered only impulsive events for this study (Figure 6 (b)) we found a negative weak correlation (-0.21) between them. We removed the outlier event lying at the right top corner of the Figure 6(b) and found that the negative correlation is increased to -0.40.

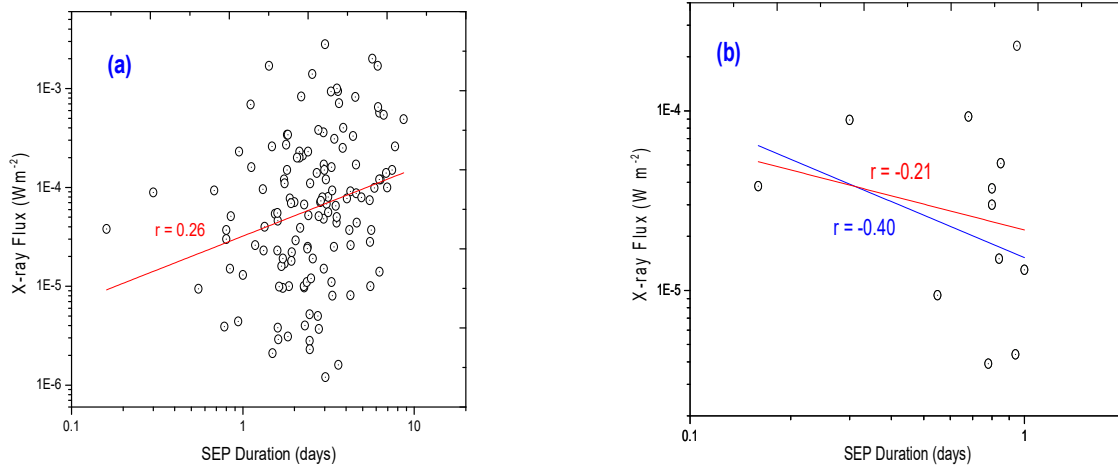


**Figure 6** Scatter plots showing correlation study of SEP duration with X-ray flux including all events (panel-a) and only impulsive SEP events (panel-b).

We also checked this correlation study for gradual events only but the correlation was decreased to 0.25. The SEP events under investigation are solar proton events and mostly associated with gradual SEP events [13, 14]. So, more impulsive events are associated with stronger GOES X-ray flux. This is because of the more and impulsive energy released during the impulsive events as well as increment in duration reflects decrement in impulsiveness. Therefore we are getting a negative correlation between them.

### 3.2 SEPs and Magnetic Complexity of Source Regions

Figure 7(a) shows the variation of magnetic configuration of associated active regions. Most of the SEP events (65 events) are associated with the active regions having the most complex magnetic configuration i.e., Hale class  $\beta\gamma\delta$ . 31 events are associated with the active regions with magnetic complexity of  $\beta$  configuration. With the active region  $\beta\gamma$ , the associated number of events is 28. Very few events are associated with the rest of the magnetic complexities (8 with  $\alpha$ , 4 with  $\beta\delta$ , 3 with  $\alpha\gamma$  and single-single events with  $\alpha\gamma\delta$  and  $\gamma\delta$ ).

Plotting the average SEP intensity against magnetic complexity classes (Figure 7(b)) revealed that  $\beta\gamma\delta$  active regions exhibited the highest average intensity, reaching 2051 pfu. It means the large SEP events are associated with these active regions having  $\beta\gamma\delta$  class of magnetic

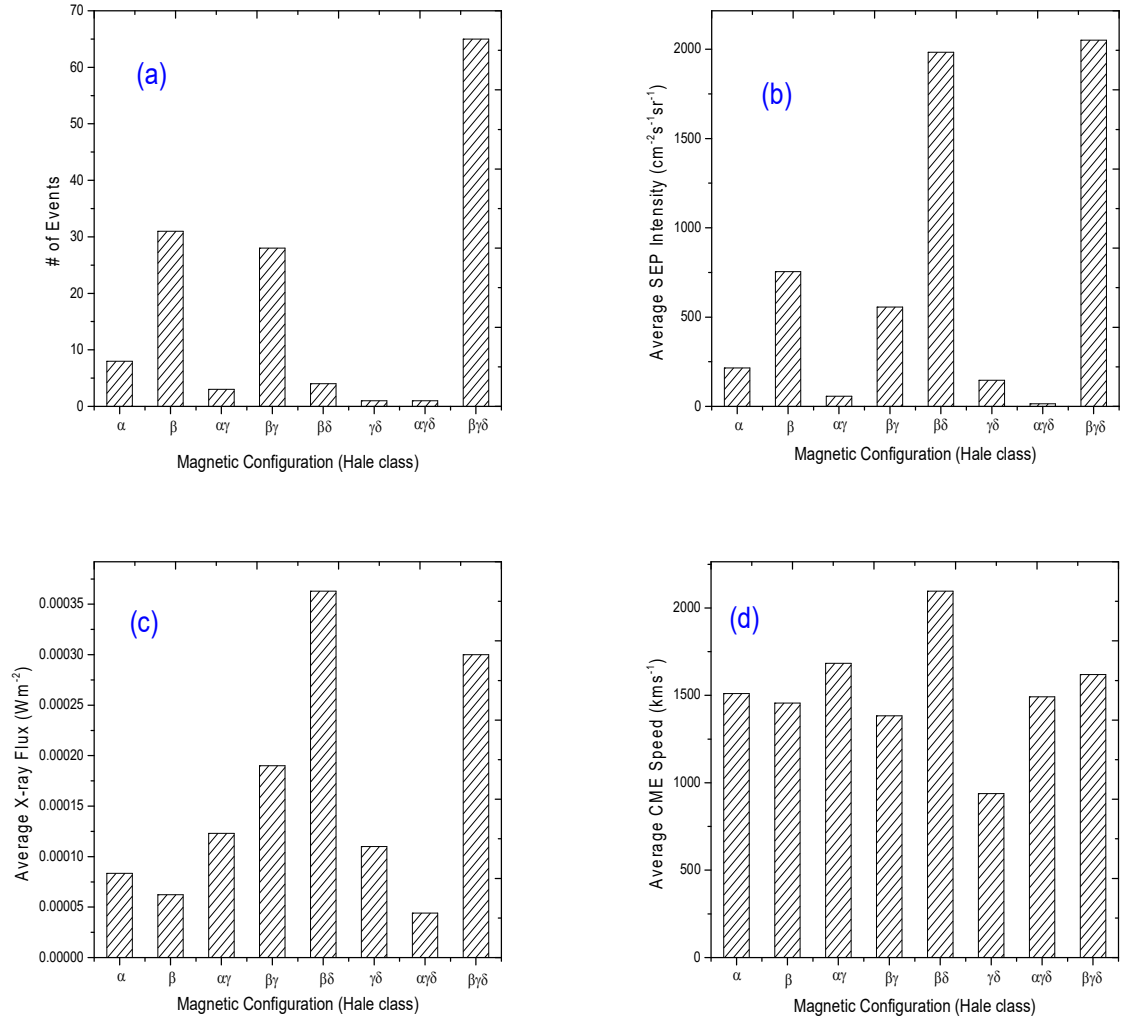


**Figure 7** Histograms showing the distribution of magnetic configuration (Hale class) with number of SEP events (panel-a), average SEP intensity (panel-b), average X-ray flux (panel-c) and average CME speed (panel-d).

complexity. Since only 4 events were associated with active regions  $\beta\delta$ , which contains one event with SEP intensity 5040 pfu. This explains why the average value comes out to be 1982 pfu. Out of these 4 events the last three events are overlapping events. This overlapping event started on 16/01/2005 and continued on 17/01/2005 as second overlapping event with SEP intensity 5040 pfu and ended in 20/01/2005 as third overlapping event. For the active regions with  $\beta$  magnetic complexity and  $\beta\gamma$  complexity, associated average SEP intensity is 754 pfu and

556 pfu respectively. Compared to the active region  $\beta$ , the average SEP intensity linked to the active region  $\alpha$  is significantly lower.

Similar results are found for the X-ray flux also (Figure 7(c)). Maximum average flux is found for the associated active regions  $\beta\gamma\delta$  and  $\beta\delta$  ( $3.00 \times 10^{-4}$  and  $3.63 \times 10^{-4} \text{ Wm}^{-2}$  respectively). So we find that those active regions which are magnetically more complex are responsible for the generation of high energetic solar flares.

Upon examining the histogram of magnetic complexity of active regions versus average CME speed (Figure 7(d)), we found that the highest average speed corresponds to active regions of the Hale class  $\beta\delta$ . This average speed is  $2096 \text{ kms}^{-1}$  and average speed of  $1618 \text{ kms}^{-1}$  is found for the magnetic configuration of  $\beta\gamma\delta$ . For the active regions having magnetic configuration of Hale class  $\alpha\gamma$ , the average speed is  $1683 \text{ kms}^{-1}$ . Minimum average speed is  $938 \text{ kms}^{-1}$ , which is associated with active regions  $\gamma\delta$ , while minimum speed of listed CME is  $296 \text{ kms}^{-1}$ . Two faster CMEs ( $2684$  and  $3163 \text{ kms}^{-1}$ ) are associated with very large active regions having complexity  $\beta\gamma\delta$ . Nine faster CMEs having speed greater than  $2500 \text{ kms}^{-1}$  are also associated with active regions having very complex magnetic configuration namely  $\beta\gamma\delta$ ,  $\beta\gamma$  and  $\beta\delta$ . This again shows the capability of large complex active regions to generate the faster CMEs as reported by Michalek and Yashiro, 2013 [29].

### 3.3 Association of SEPs with CME properties

Average CME acceleration and deceleration was plotted with magnetic complexity of solar active regions (Figure 8(a)), we found that 58 SEP events are accelerated and 82 are decelerated. Average CME acceleration is highest again for most complex Hale class of magnetic configuration, which are  $\beta\gamma\delta$  and  $\alpha\gamma\delta$ . Highest average deceleration was found corresponding to the active region  $\beta\delta$ . The maximum deceleration recorded was  $143 \text{ ms}^{-2}$ , whereas the highest CME acceleration observed was  $83 \text{ ms}^{-2}$ . All the events associated with active regions  $\alpha\gamma$  and  $\alpha\gamma\delta$  are accelerated, while all the events corresponding to active regions  $\gamma\delta$  are decelerated.

Average CME width was also plotted with magnetic complexity of solar active regions (Figure 8(b)), we found that highest average CME width was found for the magnetically most complex active regions  $\beta\delta$ ,  $\gamma\delta$ ,  $\alpha\gamma\delta$ , and the value is  $360^0$ , which means all the events associated with these active regions are also associated with halo CMEs. The average CME width corresponding to active region  $\beta\gamma\delta$  is  $346$ , which is also close to halo CMEs. This implies that larger (CME width) CMEs are mostly originated from magnetically very complex active regions.

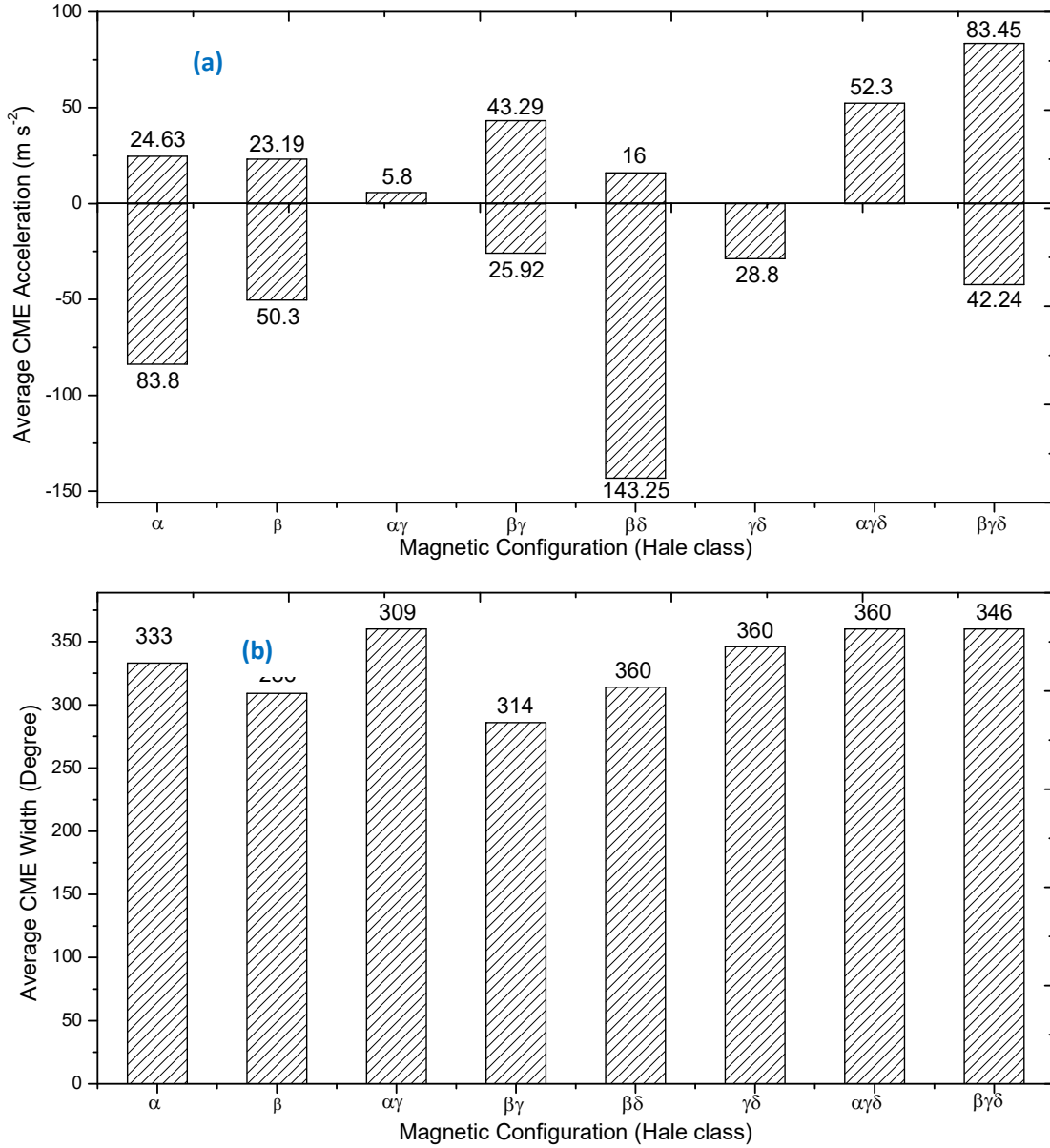


**Figure 8** Histogram of average CME acceleration and deceleration with magnetic configuration (a) and histogram of average CME width with magnetic configuration (b).

All the CMEs associated with impulsive SEP events are decelerated except two CMEs. Average CME Acceleration for impulsive events was  $-17.97 \text{ ms}^{-2}$ , while that for the gradual SEP events was  $-4.37 \text{ ms}^{-2}$ . The average CME speed associated with impulsive SEP events was  $1125 \text{ km s}^{-1}$  and  $1561 \text{ km s}^{-1}$  for the gradual events. For the gradual events, the associated CMEs are having larger width ( $327^\circ$ ) than the associated CME width ( $262^\circ$ ) for impulsive events.

### 3.4 Gradual and Impulsive events and Comparative study of Solar cycle 23 & 24

By determining the duration of each SEP event, we identified the impulsive and gradual events. The result is plotted in the panel (a) of Figure 9. We found only 10% impulsive events which are characterized as the SEP events having SEP duration of one day or less than that. Additionally, 90% of events are gradual, with SEP duration longer than a day. Although thousands of impulsive events are observed per year and few tens of gradual events are observed in a year [14-16], but we only looked at proton-rich events in our study, not electron-rich ones, which is why we found very few impulsive events.

We found that all the impulsive SEP events are originated from western hemisphere which is in well agreement with previous findings [13, 14]. We observed that all the impulsive events have SEP intensity less than 100 pfu. Many of the events are associated with C class flares or B class flares (very weak flares). We can infer from this observation that impulsive events are also associated with other solar activity features. According to Reams, 2021 [60], impulsive SEPs are also associated with magnetic reconnection in solar jets and jets with fast narrow CMEs.

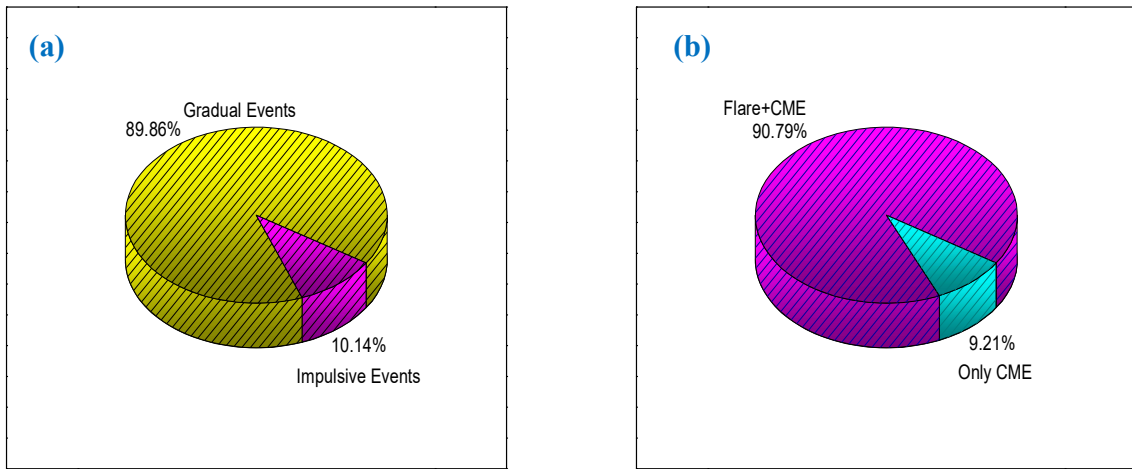


**Figure 9** Pie diagram showing the gradual versus impulsive SEP events (panel- a) and pie diagram showing events associated with flares and CMEs both versus events associated with only CMEs or CMEs and very weak flares(GOES C-class or weaker than that i.e., B-class) (panel-b).

We have characterized 10% SEP events which are associated with only CMEs or CMEs and having very weak flares i.e., C-class or B-class flares (Figure 9 (b)). We observed that maximum of these events are associated with halo CMEs and all the events are located at the limb of western hemisphere of the solar disk, only one is from the eastern limb of the solar disk. Two



impulsive SEP events are there to which the flare association is very weak. This may be because these events might be associated with solar jets also.

Solar cycles 23 and 24 are compared in table 1 to have a clear view between these two cycles. In solar cycle 23, a total of 106 SEP events were recorded, compared to only 46 events in cycle 24. Halo CMEs accounted for 75% of events in cycle 23, whereas a higher percentage (86%) was observed in cycle 24. The average SEP intensity during cycle 23 was 1524 pfu, which significantly decreased to 485 pfu in cycle 24. Similarly, the average X-ray flux dropped from  $2.33 \times 10^{-4} \text{ Wm}^{-2}$  in cycle 23 to  $1.3733 \times 10^{-4} \text{ Wm}^{-2}$  in cycle 24.

**Table 1** Comparison between solar cycle 23 and 24.

Different Activity Features	Cycle 23	Cycle 24	Total
Number of SEP Events	106	46	152
No. of Halo CMEs	73	40	113
Average SEP Intensity	1524 pfu	485 pfu	1210 pfu
Average X-ray Flux	$2.33 \times 10^{-4} \text{ Wm}^{-2}$	$1.37 \times 10^{-4} \text{ Wm}^{-2}$	$2.05 \times 10^{-4} \text{ Wm}^{-2}$
Average CME Speed	$1521 \text{ kms}^{-1}$	$1510 \text{ kms}^{-1}$	$1518 \text{ kms}^{-1}$
No. of Events in Eastern Hemisphere	20	10	30
No. of Events in Western Hemisphere	80	36	116
No. of Events in Northern Hemisphere	50	23	71
No. of Events in Southern Hemisphere	50	23	68

Average CME speed in cycle 23 is  $1521 \text{ kms}^{-1}$  and it is decreased to  $1510 \text{ kms}^{-1}$  for cycle 24. Number of SEP events in east, west, north and southern hemispheres is 20, 80, 50 and 50 respectively in case of cycle 23, while these numbers become 10, 36, 21 and 18 respectively for cycle 24. Above results clearly decide that solar cycle 24 is a weak cycle compared to cycle 23. Gopalswamy et al., 2022 [63] also revealed that sunspot numbers, high energy SEPs are less in solar cycle 24, photospheric magnetic field is also weaker in this cycle. This comparative study of solar cycle 23 and 24 can be combined with the similar kind of study for previous solar cycle. Finally these results can be used for the prediction of future solar cycle strength using the latest Artificial Intelligence technique.

#### 4. Conclusions

In this study, we have investigated 152 major SEP events associated with solar X-ray flares, CME parameters, active region characteristics and SEP durations. For this investigation, a wide range of data was collected during solar cycles 23 and 24. A summary of the study is given below.

Solar cycles 23 and 24 were compared, and it was found that cycle 24 was weaker. The average SEP intensity was 1210 pfu, indicating that most SEPs were intense. Only a few SEPs had low intensity, and these were mostly associated with impulsive events. With a 7-day SEP duration, the highest SEP intensity recorded in the dataset was 31,700 pfu, originating from an active region with the magnetic configuration  $\beta\gamma\delta$ . The linked flare belongs to the X class, and its associated CME speed exceeds  $1000 \text{ km s}^{-1}$ . The same pattern is seen in events with intensities more than 10,000 pfu, supporting previous findings that strong SEPs are caused by strong flares, large CMEs, and magnetically complex active regions.

According to a recent study by Marroquin, R., D., et al. 2023 [61], the active region  $\beta$  magnetic configuration has generated the greatest number of SEP events. The majority of the SEPs are linked to active regions  $\beta\gamma\delta$  and  $\beta$  in our study; very few events are associated with unipolar active regions. This difference may be because of the chosen SEP events. We have taken only 20 year data in an energy channel  $> 10 \text{ MeV}$  and all the SEPs are having intensity  $\geq 10$  pfu. Moreover an adequate number of SEPs are originated from the western limb of the Sun, where information about the active regions may not be reliable due to projection effects.

The average SEP intensity for the  $\beta\gamma\delta$  active region class is 2051 pfu, the highest average intensity for this configuration when compared to other magnetic active region configurations. The events that are associated to active regions  $\beta\gamma\delta$  and  $\beta\delta$  have the highest average X-ray flux. It indicates that the active regions with the most complex magnetic configuration are the ones that produce strong flares. 80% of events originate in the western hemisphere, which is consistent with earlier findings resulting from Parker's spiraling. The magnetic complexity of active regions is used to study the CME properties. We discovered that two of the faster CMEs, with respective speeds of 2684 and 3163  $\text{km s}^{-1}$ , are associated to extremely large active regions  $\beta\gamma\delta$ . The nine most rapid CMEs (with speeds above 2500  $\text{km s}^{-1}$ ) are likewise linked to active regions with extremely complex magnetic configurations  $\beta\gamma\delta$ ,  $\beta\gamma$ , and  $\beta\delta$ . Therefore, we may conclude that the production of high speed CMEs is caused by the magnetically complex active

regions. The magnetically most complicated active regions  $\beta\delta$ ,  $\gamma\delta$ ,  $\alpha\gamma\delta$ , and  $\beta\gamma\delta$  have the highest average CME width, indicating that large CMEs are a result of these active regions.

Only 10% of the major SEP events in our data set were impulsive; the remaining 90% were gradual. Since many of these impulsive events are associated with C class or very weak flares and their SEP intensity is less than 100 pfu, which indicate that impulsive events are not only caused by solar flares but also by other activity features like solar jets. The western hemisphere of the solar disk is the source of all impulsive events.

In the data set used for this study, the maximum SEP intensity is characterized as 31700 pfu. This event is a large gradual event having SEP duration of approximately 7 days. This event is, originated from the magnetically most complex active region  $\beta\gamma\delta$  [42]. Associated flare is an X-class flare and CME speed is more than  $1000 \text{ kms}^{-1}$ . This associated CME is decelerated with  $63.4 \text{ ms}^{-2}$ . All the 5 events having intensity more than 10000 pfu show similar type of behaviour. So from these results we can infer that the most intense SEP event is a consequence of the combined effect of strong X-ray flare, large CME and most complex magnetic topology. Which confirms the earlier findings and predictions that more magnetically complex regions are responsible for the generation of strong flares and CMEs hence the strong SEPs [42, 48-50].

This work leads us to the conclusion that shock-generated CMEs, solar flares associated with magnetic reconnection, and the magnetic complexity of solar active regions all contribute together to the generation of SEP events rather than being caused by a single mechanism. Both solar flares and solar jets are responsible for the impulsive events. Shocks produced by CMEs are primarily linked to gradual SEP events.

### **Acknowledgements**

We acknowledge the open data policy of NGDC, SOHO and SDO. This study made use of NASA Astrophysics Data System Bibliographic Services. We are very thankful to reviewers who gave valuable suggestions to improve the quality of paper.

### **References:**

- [1] S. E. Forbush, *Phys. Rev.*, **70**, 9 (1946)
- [2] D.V. Reames, *Space Sci. Rev.*, **175**, 53 (2013)
- [3] R. C. Carrington, *Mon Not R Astron Soc* **20**, 13 (1859)
- [4] K.L. Klein and S. Dalla, *Space Sci Rev.*, **212**, 1107 (2017)
- [5] S. W., Kahler, E. Hildner Van Hollebeke MAI, *Sol. Phys.* **57**, 429 (1978)
- [6] S.W. Kahler, N.R. Jr. Sheeley, R.A. Howard *et al.*, *J. Geophys. Res.* **89**, 9683 (1984)

- [7] E. W. Cliver, S. W. Kahler, M. A. Shea, D. F. Smart, *Astrophys J.*, **260**, 362 (1982)
- [8] G. E. Kocharov, *In: International cosmic ray conference*, **12**, 235 (1983)
- [9] A. Luhn, B. Klecker, D. Hovestadt *et al.*, *Adv. Space Res.*, **4**, 161 (1984)
- [10] G.M. Mason, G. Gloeckler, D. Hovestadt, *Astrophys. J.*, **280**, 902 (1984)
- [11] H. V. Cane, R. E. McGuire, T. T. von Rosenvinge, *Astrophys J.*, **301**, 448 (1986)
- [12] D. V. Reames, *Astrophys. J. Lett.*, **330**, 71 (1988)
- [13] D.V. Reames, *Space Sci. Revs.* **90**, 413 (1999)
- [14] M. Desai, and J. Giacalone, *Liv. Rev. Sol. Phys.* **13(1)**, 3 (2016)
- [15] D.V. Reames, *Rev. Geophys.*, **33(S1)**, 585 (1995)
- [16] M.B. Kallenrode, *J. Phys.G: Nuclear and Particle Phys.*, **29(5)**, 965 (2003)
- [17] D.V. Reames, T.T. Von Rosenvinge, R.P., Lin, *The Astrophys. J.*, **292**, 716 (1985)
- [18] E.W. Cliver, *In AIP Conference Proceedings, American Inst. Phys*, **528 (1)**, 21 (2000)
- [19] N. Gopalswamy, S. Yashiro, S. Akiyama, *J. Geophys. Res.*, **112**, 6112 (2007)
- [20] N. Gopalswamy, S. Yashiro, S. Akiyama, *et al.*, *Ann. Geophys.* **26**, 3033 (2008)
- [21] J.F. Drake, P.A. Cassak, M.A., Shay *et al.*, *Astrophys. J. Lett.* **700**, 16 (2009)
- [22] D.V. Reames, *Space Sci. Rev.*, **194(1-4)**, 303 (2015)
- [23] D.V. Reames, *Sol. Phys.*, **297(3)**, 32 (2022)
- [24] J. Giacalone, *Astrophys. J.*, **761(1)**, 28 (2012)
- [25] D.V. Reames, , *The Astrophys. J.*, **757(1)**, 93 (2012)
- [26] N. Gopalswamy, P. Makela, S. Akiyama *et al.*, *Sun and Geosphere*, **10(2)**, 111 (2015)
- [27] N. Gopalswamy, H. Xie, S.Akiyama *et al.*, , *Earth, Planets and Space*, **66**, 1, (2014)
- [28] R. Kumar, R. Chandra, B. Pande, *et al.*, *J. Astrophys. & Astr.*, **41**, 1 (2020)
- [29] S.W. Kahler, *J. Geophys. Res.: Space Phys.*, **106(A10)**, 20947 (2001)
- [30] N. Gopalswamy, S. Yashiro, S. Krucker *et al.*, *J. Geophys. Res.: Space Phys.* **109**, (2004)
- [31] H.V.Cane, I.G. Richardson, T.T. von Rosenvinge, *J. Geophys. Res.* **115**, 8101 (2010)
- [32] E.W. Cliver, A.G. Ling, A. Belov, S. Yashiro, *Astrophys. J. Lett.* **756**, 29 (2012)
- [33] I.G. Richardson, T.T. von Rosenvinge, H.V. Cane, *et al.*, *Sol. Phys.*, **289**, 3059 (2014)
- [34] N. Gopalswamy, S. Yashiro, G. Michalek *et al.*, *Earth, Moon, and Planets*, **104**, 295 (2009)
- [35] G.M. Mason, J.E. Mazur, J.R. Dwyer, *The Astrophys. J.*, **525(2)**, L133 (1999)
- [36] R. Miteva, K.L. Klein, O. Malandraki, *et al.*, *Sol. Phys.*, **282**, 579 (2013)
- [37] N. Gopalswamy, S.Yashiro, A. Lara, *et al.*, *Geophys. Res. Lett.*, **30(12)**, 8015 (2003)
- [38] G.Trottet, , Samwel, S., Klein, K.L. *et al.*, *Sol. Phys.*, **290**, 819 (2015)
- [39] B. Klecker, E. Mbius, M.A. Popecki, *Space Sci. Rev.* **130**, 273 (2007)

- [40] E.W. Cliver, In: Proceedings of the International Astronomical Union, 4, Symposium S257, **401C**, (2009)
- [41] J.K. Thalmann, Y. Su, M. Temmer, *et al.*, *The Astrophys. J. Lett.*, **801(2)**, L23 (2015)
- [42] K. Bronarska and G. Michalek, *Adv. Space Res.*, **59(1)**, 384 (2017)
- [43] P.K. Mitra, B. Joshi, A. Prasad *et al.*, *The Astrophys. J.*, **869(1)**, 69 (2018)
- [44] A. Bruno, E.R. Christian, G.A. De Nolfo *et al.*, *Space Weather*, **17(3)**, 419 (2019)
- [45] L.K. Kashapova, R. Miteva, I.N. Myagkova *et al.*, *Sol. Phys.*, **294(1)**, 9 (2019)
- [46] H. Zirin, M.A. Liggett, *Sol. Phys.* **113**, 267 (1987)
- [47] I. Sammis, F. Tang, H. Zirin, *The Astrophys. J.*, **540(1)**, 583 (2000)
- [48] Y. Liu, D.F. Webb, X.P. Zhao, *The Astrophys. J.*, **646(2)**, 1335 (2006)
- [49] G. Michalek, S. Yashiro, *Adv. Space Res.*, **52(3)**, 521 (2013)
- [50] L.K. Kashapova, A.V. Zhukova, R. Miteva, *et al.*, *Geomagnetism and Aeronomy*, **61**, 1022 (2021)
- [51] S. Yashiro, N. Gopalswamy, G. Michalek, *et al.*, *Journal of Geophysical Research: Space Physics*, **109(A7)** (2004)
- [52] G.E. Brueckner, R.A. Howard, M.J. Koomen *et al.*, *The SOHO mission*, **357** (1995)
- [53] G.E. Hale., F. Ellerman, S.B. Nicholson *et al.*, *Astrophysical Journal*, **49**, 153 (1919)
- [54] S.A. Jaeggli, A.A. Norton, *The Astrophys. J. Lett.*, **820(1)**, L11 (2016)
- [55] S. Dalla, In *AIP Conference Proceedings*, **679**, 660 (2003)
- [56] K. Kecskeméty, E.I. Daibog, Y.I. Logachev *et al.*, *Journal of Geophysical Research: Space Physics*, **114(A6)** (2009)
- [57] A. García-Rigo, M. Núñez, R. Qahwaji *et al.*, *J. Spac. Weath. Spac. Clim.*, **6**, A28 (2016)
- [58] K.A. Firoz, W.Q. Gan, Y.P. Li *et al.*, *Solar Physics*, **297(6)**, 71 (2022)
- [59] L. Will, E.A. Avallone, X. Sun, *Res. NAAS*, **6(2)**, 37 (2022)
- [60] D.V. Reames, *Space Sci. Rev.*, **217(6)**, 72 (2021)
- [61] R. D. Marroquin, V. Sadykov, A. Kosovichev, *et al.*, *The Astrophys. J.*, **952**:97,10 (2023)
- [62] H. Künzel, , Zur Klassifikation von Sonnenfleckengruppen. *Astronomische Nachrichten*, 288, 177 (1965)
- [63] N. Gopalswamy, P. Mäkelä, S. Yashiro *et al.*, *J. of Phys.: Conf. Ser.* **2214**, 012021 (2022)

### Statements and Declarations:

**Funding** – We declare that no funding, grants or other support were received during the preparation of this manuscript.

**Competing Interests** - *The authors have no relevant financial or non-financial interests to disclose.*

**Author Contributions** – *All authors contributed in this study equally. Material preparation and data collection was performed by Raj Kumar and Ramesh Chandra. Analysis was performed by all the authors viz. Raj Kumar, Ramesh Chandra, Bimal Pande and Seema Pande. First and corresponding author has written the first draft of the manuscript and all the authors commented and contributed to make it final.*

**Appendix: Supplementary Information: Table 2.**

Day	start time hours	End date & time	SEP duration days	SEP (pfu)	CME						Flare class	NOAA Active Region Number	hale class	Total Sunspot Area present in the active region	Number of spots
					Day	time	Accelera tion	speed	width	location					
04-11-97	6.66	06-11-97 12.5 h	2.24	72	04-11-97	6:10	-22.10	785	H	S14W33	X2.1/2B	8100	$\beta\gamma\delta$	660	34
06-11-97	12.5	10-11-97 2.6h	3.59	495	06-11-97	12:10	-44.10	1556	H	S18W63	X9.4/2B	8100	$\beta\gamma\delta$	900	19
20-04-98	11.25	26-04-98 17.77h	6.27	1700	20-04-98	10:07	43.50	1863	>243	S22W90	M1.4/--	(8205)8194	$\beta$	70	12
02-05-98	14	05-05-98 1.33 h	2.47	146	02-05-98	14:06	-28.80	938	H	S15W15	X1.1/3B	8210	$\gamma\delta$	340	30
06-05-98	8.42	08-05-98 3.55 h	1.79	207	06-05-98	8:29	24.50	1099	190	S11W65	X2.7/1N	8210	$\beta$	480	
09-05-98	6.33	11-05-98 3.55 h	1.88	11	09-05-98	3:35	140.50	2331	178	S14W89	M7.7/--	8214	$\beta$	380	21
24-08-98	23.17	No data		665	No data					N35E09	X1.0/3B	8307	$\beta\delta$	450	12
23-09-98	14.33	25-09-98 14.22h	2.00	44	No data					N18E09	M7.1/3B	No data			
30-09-98	14.33	No data		1160	No data					N23W81	M2.8/2N	8340	$\alpha$	230	1
07-11-98	22.42	08-11-98 11.55h	0.55	11	07-11-98	20:54	23.70	750	321		C9.4	8375	$\beta\gamma\delta$	410	41
14-11-98	6.5	No data		314	No data					N28W90	C1.3/--	8375(8383)	$\beta$	90	10
20-01-99	22.83			14						N27E90	M5.2/--	8439	$\beta\gamma$	300	44
24-04-99	15.5	26-04-99 15.11h	1.98	32	24-04-99	13:31	37.10	1495	H	>NW90		8516	$\beta$	30	8
04-05-99	3	07-05-99 15.55h	3.52	14	03-05-99	6:06	15.80	1584	H	N15E32	M4.4/2N	8525/8524	$\beta$	290	16
01-06-99	21	04-06-99 08.00h	2.45	48	01-06-99	19:37	1.80	1772	H	>NW90	C2.8	8552	$\beta$	150	11
04-06-99	8.0	06-06-99 12.22h	2.16	64	04-06-99	7:26	-158.80	2230	150	N17W69	M3.9/2B	8552	$\beta$	290	5
18-02-00	10.08	19-02-00 10 h	1.00	13	18-02-00	9:54	-9.60	890	118	>NW90	C1.3/--	8872	$\beta$	20	6
04-04-00	17	06-04-00 23.77h	2.28	55	04-04-00	16:32	12.80	1188	H	N16W66	C9.4	8933	$\beta$	240	16
06-06-00	22.33	09-06-00 08.00h	2.40	84	06-06-00	15:54	1.50	1119	H	N20E18	X2.3/--	9026	$\beta\gamma\delta$	820	22
10-06-00	17.66	13-06-00 3.55 h	2.41	46	10-06-00	17:08	-21.20	1108	H	N22W38	M5.2/3B	9026	$\beta\gamma$	400	33
14-07-00	10.58	20-07-00 16.88h	6.26	2400 0	14-07-00	10:54	-96.10	1674	H	N22W07	X5.7/3B	9077	$\beta\gamma\delta$	730	42
22-07-00	12.42	23-07-00 07.55h	0.80	17	22-07-00	11:54	-12.40	1230	105	N14W56	M3.7/2N	9085	$\beta$	190	18
28-07-00	1.75	30-07-00 12.88h	2.46	12	27-07-00	19:54	-21.40	905	H	>N90	C2.3	9097	$\beta\gamma$	250	23
11-08-00	14.5	11-08-00 21.33h	0.28	17	11-08-00	1:31	4.50	296	95	No data		9114	$\beta\gamma$	300	19
12-09-00	13.83	18-09-00 3.11 h	5.55	321	12-09-00	11:54	58.20	1550	H	S19W06	M1.0/2N	9154	$\beta$	120	5
16-10-00	8.17	19-10-00 17.77h	3.40	15	16-10-00	7:27	9.90	1336	H	N03W90	M2.5/--	9192	$\beta$	20	6
25-10-00	13.58	27-10-00 20.88h	2.30	15	25-10-00	8:26	17.40	770	H	N09W63	C4.0/--	9198	$\beta$	110	5
08-11-00	23.58	14-11-00 11.55h	5.50	1480 0	08-11-00	23:06	69.90	1738	>170	N10W77	M7.4/3F	9213	$\beta$	120	5
24-11-00	5.32	25-11-00 4.00 h	0.95	94	24-11-00	15:30	-3.30	1245	H	N22W07	X2.3/2B	9236	$\beta$	390	17
25-11-00	4	29-11-00 0.44 h	3.85	942	26-11-00	17:06	5.80	980	H	No data	X4.0	9236	$\beta\gamma$	580	29
28-01-01	17.25	31-01-01 16.44h	2.97	49	28-01-01	15:54	3.50	916	250	S04W59	M1.5/1N	9313	$\beta$	30	7
29-03-01	12.25	01-04-01 11.55h	2.97	35	29-03-01	10:26	3.50	942	H	N20W19	X1.7/1F	9393	$\beta\gamma\delta$	2240	51
02-04-01	23.17	08-04-01 16.00h	5.70	1110	02-04-01	22:06	108.50	2505	244	N19W72	X20./--	9393	$\beta\gamma\delta$	1700	53



10-04-01	8.25	12-04-01 11.66h	2.14	355	10-04-01	5:30	211.60	2411	H	S23W09	X2.3/3B	9415	$\beta\gamma\delta$	760	32
12-04-01	11.66	14-04-01 15.11h	2.14	51	12-04-01	10:31	-20.00	1184	H	S19W43	X2.0/--	9415	$\beta\gamma\delta$	550	23
15-04-01	14	18-04-01 3.00 h	2.54	951	15-04-01	14:06	-35.90	1199	167	S20W85	X14./2B	9415	$\beta\gamma$	360	9
18-04-01	3	20-04-01 15.11h	2.50	321	18-04-01	2:30	-9.50	2465	H	>SW90	No Flare	9415	$\beta\gamma$	20	2
27-04-01	1.08	28-04-01 19.11h	1.75	57	26-04-01	12:30	21.10	1006	H	N20W05	M1.7/--	9433	$\beta\gamma\delta$	1070	82
07-05-01	14	09-05-01 4.44h	1.60	30	07-05-01	12:06	19.20	1223	205	>NW90	C3.8	9447	$\beta\gamma$	200	6
15-06-01	16.42	18-06-01 4.00 h	2.48	27	15-06-01	15:56	56.90	1701	H	>SW90	No Flare	9487	$\beta\gamma$	140	3
09-08-01	19.5	11-08-01 15.55h	1.83	17	09-08-01	10:30	4.40	479	175	N11W14	C3.1	9557	$\beta\gamma$	270	11
16-08-01	0.75	19-08-01 09.33h	3.36	493	15-08-01	23:54	-31.70	1575	H	>SW90	No Flare	9573	$\beta\gamma\delta$	40	5
15-09-01	12.08	16-09-01 8.22 h	0.84	12	15-09-01	11:54	-4.00	478	130	S21W49	M1.5/1N	9608	$\beta\gamma\delta$	1020	34
24-09-01	11.66	01-10-01 12.4 h	7.74	1290 0	24-09-01	10:30	54.10	2402	H	S16E23	X2.6/--	9632	$\beta\gamma\delta$	780	17
01-10-01	12.25	05-10-01 18 h	4.24	2360	01-10-01	5:30	97.80	1405	H	S24W81	M9.1/--	9628	$\beta\gamma\delta$	800	20
19-10-01	18	20-10-01 20.88h	1.12	12	19-10-01	16:50	-0.70	901	H	N15W29	X1.6/2B	9661	$\beta\gamma\delta$	660	24
22-10-01	16.75	24-10-01 23.55h	2.28	24	22-10-01	15:06	-8.00	1336	H	S21E18	M6.7/2N	9672	$\beta\gamma\delta$	330	14
04-11-01	16.66	11-11-01 15.55h	6.95	3170 0	04-11-01	16:35	-63.40	1810	H	N06W18	X1.0/3B	9684	$\beta\gamma\delta$	440	27
17-11-01	8.83	22-11-01 21.4 h	5.52	34	17-11-01	5:30	-22.50	1379	H	S13E42	M2.8/1N	9704	$\beta\gamma\delta$	430	14
22-11-01	21.25	23-11-01 1.083h	0.16	25	22-11-01	20:30	-43.30	1443	H	S25W67	M3.8/2B	9704	$\beta\gamma\delta$	560	30
23-11-01	1.08	28-11-01 21.77h	5.86	4800	22-11-01	23:30	-12.90	1437	H	S17W36	M9.9/--	9710	$\beta\gamma\delta$	560	30
26-12-01	5.83	29-12-01 1.83h	2.83	780	26-12-01	5:30	-39.90	1446	212	N08W54	M7.1/1B	9742	$\beta\gamma$	1070	49
29-12-01	1.83	30-12-01 21.42h	1.81	76	28-12-01	20:30	6.90	2216	H	S26E90	X3.4/--	9756/9767	$\alpha\gamma$	70	1
30-12-01	21.42	07-01-02 15.11h	7.74	108	30-12-01	23.3	-10.20	457	H	No data		9754	$\beta\gamma$	160	28
10-01-02	8.66	14-01-02 5.583h	3.87	92	08-01-02	17:54	81.40	1794	H	>NE90	No data	9778	$\beta\gamma\delta$	170	9
14-01-02	5.58	18-01-02 20.44h	4.62	15	14-01-02	5:35	52.30	1492	H	S28W83	M4.4/--	9772	$\alpha\gamma\delta$	30	1
20-02-02	6.75	21-02-02 3.11h	0.85	13	20-02-02	6:30	-17.10	952	H	N12W72	M5.1/1N	9825	$\beta\gamma$	210	11
16-03-02	8.42	18-03-02 6.75 h	1.93	13	15-03-02	23:06	-17.40	957	H	S08W03	M2.2/1F	9866	blank	690	26
18-03-02	6.75	20-03-02 13.33h	2.27	53	18-03-02	2:54	-2.90	989	H	S10W30	M1.0/--	9866	$\beta\gamma\delta$	470	24
20-03-02	13.33	21-03-02 12.88h	0.98	20	20-03-02	14:54	-5.89	439.5	27	No data		9866	$\beta\gamma\delta$	290	10
22-03-02	13.83	24-04-02 6.22h	1.68	16	22-03-02	11:06	-22.50	1750	H	S09W90	M1.6/--	9866	$\beta\gamma\delta$	190	1
17-04-02	11.58	18-04-02 16.0h	1.18	24	17-04-02	8:26	-19.80	1240	H	S14W34	M2.6/2N	9906	$\beta\gamma\delta$	590	27
21-04-02	1.75	28-04-02 12h	7.43	2520	21-04-02	1:27	-1.40	2393	H	S14W84	X1.5/1F	9906	$\beta\gamma$	680	27
22-05-02	7.17	25-05-02 0.88 h	2.74	820	22-05-02	3:50	-10.40	1557	H	S30W34	C5.0/--	9954	$\beta\gamma\delta$	90	8
07-07-02	12.75	09-07-02 9.33h	1.86	23	07-07-02	11:30	22.00	1423	>228	S19W90	M1.0/--	17	$\beta$	40	2
16-07-02	10.25	19-07-02 8.33 h	1.92	234	15-07-02	21:30	-7.30	1300	>188	N19W01	M1.8/--	30	$\beta\gamma\delta$	780	71
19-07-02	8.33	20-07-02 3.11 h	0.78	14	No Data			Sever al CME s	No Data		c3.9	30	$\beta\gamma\delta$	1060	83
21-07-02	3.33	25-07-02 12.88h	4.40	28	20-07-02	22:06	No data	1941	H	S13E90	X3.3/--	36	$\beta\gamma\delta$	880	26
14-08-02	2.83	15-08-02 16.88h	1.59	26	14-08-02	2:30	-0.20	1309	133	N09W54	M2.3/1N	61	$\beta\gamma$	80	6
22-08-02	2.66	23-08-02 15.55h	1.54	36	22-08-02	2:06	-32.80	998	H	S07W62	M5.4/2B	69	$\beta\gamma\delta$	1650	46
24-08-02	1.5	27-08-02 11.55h	3.42	317	24-08-02	1:27	43.70	1913	H	S02W81	X3.1/1F	69	$\beta\gamma\delta$	830	17

06-09-02	3.83	08-09-02 14.66h	2.45	208	05-09-02	16:54	43.00	1748	H	N09E28	C5.2/SF	102	$\alpha$	20	1
09-11-02	15.42	11-11-02 5.77 h	1.60	404	09-11-02	13:31	35.40	1838	H	S12W29	M4.6/2B	180	$\beta\gamma\delta$	600	58
28-05-03	4.25	31-05-03 3.00h	2.95	121	28-05-03	0:50	25.90	1366	H	S07W20	X3.6/--	365	$\beta\gamma\delta$	400	38
31-05-03	3	31-05-03 19.33h	0.68	27	31-05-03	2:30	-2.40	1835	H	S07W65	M9.3/2B	365	$\beta\gamma\delta$	800	25
18-06-03	9.25	21-06-03 11.11h	3.08	24	17-06-03	23:18	-2.90	1813	H	S07E55	M6.8/--	386	$\beta$	190	13
26-10-03	18	28-10-03 11.75h	1.74	466	26-10-03	17:54	4.80	1537	>171	N02W38	X1.2/1N	484	$\beta\gamma\delta$	1700	52
28-10-03	11.75	29-10-03 21.92h	1.42	2950 0	28-10-03	11:30	-105.20	2459	H	S16E08	X17./--	486	$\beta\gamma\delta$	2180	74
29-10-03	21.92	02-11-03 10.92h	3.54	3300	29-10-03	20:54	-146.50	2029	H	S15W02	X10./2B	486	$\beta\gamma\delta$	2120	55
02-11-03	10.92	02-11-03 17.58h	0.28	30	02-11-03	9:30	-64.20	2036	H	>SW90	X9	No data			
02-11-03	17.58	04-11-03 22.25h	2.19	1570	02-11-03	17:30	-32.40	2598	H	S14W56	X8.3/2B	486	$\beta\gamma\delta$	1900	99
04-11-03	22.25	07-11-03 22.66h	3.02	353	04-11-03	19:54	434.80	2657	H	S19W83	X28./3B/ X18	486	$\beta\gamma\delta$	1430	16
21-11-03	16.5	23-11-03 0.02h	1.31	14	20-11-03	8:06	-44.70	669	H	N01W08	M9.6/2B	501	$\beta\gamma\delta$	340	15
02-12-03	12.42	05-12-03 20.22h	3.33	89	02-12-03	10:50	18.50	1393	>150	S11W90	C8.0/--	508	$\beta$	140	8
11-04-04	6.17	12-04-04 23.11h	1.71	35	11-04-04	4:30	-77.60	1645	314	S14W47	C9.6/1F	588	$\beta$	150	10
25-07-04	16.92	28-07-04 23.77h	3.29	2090	25-07-04	14:54	7.00	1333	H	N08W33	M1.1/1F	652	$\beta\gamma\delta$	1610	73
13-09-04	20	16-09-04 19.11h	2.96	273	12-09-04	0:36	22.50	1328	H	N03E49	M4.8/2N	672	$\beta\gamma$	260	49
19-09-04	18.17	21-09-04 11.11h	1.71	57	No data					N03W58	M1.9/--	672	$\beta$	100	16
01-11-04	6.17	02-11-04 20.88h	1.61	63	01-11-04	6:06	-29.70	925	146	>NW90	c2.9	687	$\beta$	60	4
07-11-04	18.42	09-11-04 20.00h	2.07	495	07-11-04	16:54	-19.70	1759	H	N09W17	X2.0/--	696	$\beta\gamma\delta$	910	33
09-11-04	20	10-11-04 3.25h	0.30	82	09-11-04	17:26	-65.10	2000	H	N08W51	M8.9/2N	696	$\beta\gamma\delta$ /	600	48
10-11-04	3.25	13-11-04 23.11h	3.83	424	10-11-04	2:26	-108.00	3387	H	N09W49	X2.5/3B	696	$\beta\gamma\delta$	730	37
16-01-05	1.08	17-01-05 12.66h	1.48	365	15-01-05	23:06	-127.40	2861	H	N15W05	X2.6/--	720	$\beta\delta$	1540	23
17-01-05	12.66	20-01-05 06.92h	2.76	5040	17-01-05	9:54	-159.10	2547	H	N15W25	X3.8/--	720	$\beta\delta$	1630	37
20-01-05	6.92	23-01-05 22.44h	3.64	1860	20-01-05	6:54	16.00	882	H	N14W61	X7.1/2B	720	$\beta\delta$ /	1220	31
13-05-05	18.75	16-05-05 22.44h	3.15	3140	13-05-05	17:12	No data	1689	H	N12E11	M8.0/2B	759	$\beta$	300	10
16-06-05	20.75	18-06-05 04.88h	1.34	44	No data					N08W90	M4.0/SF	775	$\beta$	230	4
14-07-05	13.08	17-07-05 14.25h	3.05	134	14-07-05	10:54	198.00	2115	H	N11W90	X1.2/--	786	$\beta\gamma\delta$	370	8
17-07-05	14.25	19-07-05 15.33h	2.05	22	17-07-05	11:30	59.20	1527	H	>NW90	No data				
27-07-05	22.42	02-08-05 13.11h	5.61	41	27-07-05	4:54	-75.40	1787	H	N11E90	M3.7/--	791	$\beta$	160	19
22-08-05	19.33	25-08-05 22.88h	3.15	337	22-08-05	17:30	108.00	2378	H	S13W65	M5.6/1N	798	$\beta\gamma$	560	18
07-09-05	20.17	13-09-05 23.00h	6.12	1880	No data					S11E77	X17./3B	808	$\beta\gamma$	10	1
13-09-05	23	16-09-05 22.66h	2.99	183	13-09-05	20:00	11.50	1866	H	S09E10	X1.5/2B	808	$\beta\gamma\delta$	840	52
06-12-06	23.25	13-12-06 02.92h	6.15	1980	06-12-06	20:12	No data		H	S05E64	X6.5/3B	930	$\beta$	390	5
13-12-06	2.92	14-12-06 22.92h	1.83	698	13-12-06	2:54	-61.40	1774	H	S06W23	X3.4/4B	930	$\beta\gamma\delta$	680	17
14-12-06	22.92	16-12-06 18.44h	1.81	215	14-12-06	22:30	-0.40	1042	H	S06W46	X1.5/--	930	$\beta\gamma\delta$	670	11
14-08-10	11.08	15-08-10 09.55h	0.94	14	14-08-10	10:12	-43.00	1205	H	N17W52	C4.4/--	1099	$\beta$	10	13
07-03-11	21.75	12-03-11 02h	4.18	50	07-03-11	20:00	-63.10	2125	H	N31W53	M3.7/--	1164	$\beta\gamma\delta$	640	25
21-03-11	4.17	22-03-11 19.11h	1.62	14	21-03-11	2:24	8.00	1341	H	>W90	1169		No Data		
07-06-11	7.33	09-06-11 16.66h	2.39	72	07-06-11	6:49	0.30	1255	H	S21W54	M2.5/2N	1226	$\beta$	80	8
04-08-11	4.5	07-08-11 12.22h	3.32	96	04-08-11	4:12	-41.10	1315	H	N19W36	M9.3/2B	1261	$\beta\gamma\delta$	300	15

09-08-11	8.33	10-08-11 10.88h	1.11	26	09-08-11	8:12	-40.60	1610	H	N17W69	X6.9/2B	1263		$\beta\gamma\delta$	450	13
22-09-11	17.92	29-09-11 14.66h	6.86	35	22-09-11	10:48	-68.30	1905	H	N09E89	X1.4/--	1302		$\beta\gamma$	480	2
26-11-11	8.25	29-11-11 8.88h	3.03	80	26-11-11	7:12	9.00	933	H	N17W49	C1.2/--	1353		$\alpha\gamma$	10	1
23-01-12	4.75	27-01-12 18.92h	4.59	6310	23-01-12	4:00	28.00	2175	H	N28W21	M8.7/--	1402		$\beta\gamma$	370	8
27-01-12	18.92	01-02-12 8.88h	4.58	795	27-01-12	18:27	165.90	2508	H	N27W71	X1.7/1F	1402		$\beta\gamma$	270	9
07-03-12	2.83	13-03-12 18.08h	6.63	6530	07-03-12	0:24	-88.20	2684	H	N17E27	X5.4/--	1429		$\beta\gamma\delta$	1120	25
13-03-12	18.08	16-03-12 16.00h	2.91	469	13-03-12	17:36	45.60	1884	H	N17W66	M7.9/--	1429		$\beta\gamma\delta$	380	14
17-05-12	1.92	19-05-12 20.44h	2.77	255	17-05-12	1:48	-51.80	1582	H	N11W76	M5.1/1F	1476		$\beta\gamma\delta$	230	3
26-05-12	23.42	28-05-12 14.22h	1.62	14	26-05-12	20:57	-159.20	1966	H	>W90		No data				
14-06-12	23.42	17-06-12 12.88h	2.56	15	14-06-12	14:12	-1.20	987	H	S17E06	M1.9/1N	1504		$\beta\gamma\delta$	560	25
07-07-12	0.08	08-07-12 18.17h	1.75	25	06-07-12	23:24	-56.10	1828	H	S13W59	X1.1/--	1515		$\beta\gamma\delta$	670	56
08-07-12	18.17	10-07-12 16.22h	1.91	19	08-07-12	16:54	-117.20	1497	157	S17W74	M6.9/1N	1515		$\beta\gamma$	780	43
12-07-12	17.42	15-07-12 10.22h	2.70	96	12-07-12	16:48	195.60	885	H	S15W01	X1.4/--	1520		$\beta\gamma\delta$	1320	48
17-07-12	15.5	19-07-12 6.66h	1.63	136	17-07-12	13:48	63.50	958	176	S28W65	C9.9/1F	1520		$\beta\gamma\delta$	430	12
19-07-12	6.66	23-07-12 8.00h	4.05	80	19-07-12	5:24	-8.00	1631	H	S13W88	M7.7/--	1520		$\beta\gamma\delta$	300	5
23-07-12	8	26-07-12 19.33h	3.47	12	23-07-12	2:36	-24.60	2003	H	>W90		No data				
01-09-12	1.42	05-09-12 7.11h	4.24	60	31-08-12	20:00	2.00	1442	H	S25E59	C8.1/2F	1562		$\alpha$	10	1
28-09-12	1.33	30-09-12 20.00h	2.78	28	28-09-12	0:12	-27.10	947	H	N06W34	C3.7/1F	1577		$\beta\gamma$	15	3
15-03-13	19.66	18-03-13 4.22h	2.36	16	15-03-13	7:12	25.80	1063	H	N11E12	M1.1/1F	1692		$\alpha$	200	2
11-04-13	8.42	14-04-13 20.00h	3.48	114	11-04-13	7:24	-8.10	861	H	N09E12	M6.5/3B	1719		$\beta\gamma$	190	17
15-05-13	6.58	21-05-13 15.33h	6.36	42	15-05-13	1:48	-52.10	1366	H	N12E64	X1.2/2N			$\beta\gamma\delta$	310	5
22-05-13	14.33	26-05-13 3.11h	3.53	1660	22-05-13	13:25	-13.20	1466	H	N15W70	M5.0/--	1745		$\beta\gamma\delta$	120	5
23-06-13	8.5	25-06-13 9.11h	2.03	14	21-06-13	3:12	1.50	1900	>207	S16E73	M2.9/--	1778		$\alpha\gamma$	110	1
30-09-13	0.42	03-10-13 15.11h	3.61	182	29-09-13	22:12	-5.30	1179	H	N17W29	C1.6/--	1850		$\beta\gamma$	100	7
28-12-13	19	30-12-13 17.33h	1.93	29	28-12-13	17:36	-26.70	1118	H	>W90	C9	1936				
06-01-14	8.25	07-01-14 19.92h	1.49	42	06-01-14	8:00	-7.10	1402	H	>W90	C2.1/--	1936/1937		$\beta\gamma$	160	21
07-01-14	19.92	14-01-14 2.00h	6.25	1026	07-01-14	18:24	-60.80	1830	H	S15W11	X1.2/--	1944		$\beta\gamma\delta$	1415	11
20-02-14	8.25	21-02-14 3.55h	0.80	22	20-02-14	8:00	-9.50	948	H	S15W73	M3.0/--	1976		$\alpha$	180	5
25-02-14	3.83	05-03-14 20.00h	8.67	24	25-02-14	1:25	-158.10	2147	H	S12E82	X4.9/--	1990		$\alpha$	250	2
18-04-14	13.66	21-04-14 10.00h	2.85	58	18-04-14	13:25	13.50	1203	H	S20W34	M7.3/--	2036		$\beta\gamma$	510	34
10-09-14	21.58	14-09-14 4.44h	3.29	126	10-09-14	18:00	-51.60	1267	H	N14E02	X1.6/--	2158		$\beta\gamma\delta$	420	25
01-11-14	13.92	04-11-14 6.44h	2.69	11	01-11-14	6:00	-1.00	740	>160	N27W79		No data				
18-06-15	4.58	20-06-15 16.66h	2.50	17	18-06-15	1:25	27.70	1714	195	S16W81	M1.2/--	2365		$\alpha$	60	1
21-06-15	4.08	25-06-15 10.08h	4.25	1066	21-06-15	2:36	21.20	1366	H	N12E16	M2.6/--	No data				
25-06-15	10.08	30-06-15 8.22h	4.92	22	25-06-15	8:36	-24.80	1627	H	N09W42	M7.9/--	2371		$\beta\gamma$	740	29
29-10-15	3.08	30-10-15 20.66h	1.73	24	29-10-15	2:36	-7.50	530	202	>W90b		2434		No data		
02-01-16	0.25	03-01-16 08.00h	1.32	22	01-01-16	23:24	12.70	1730	H	S25W82	M2.3/--	2473		$\beta$	130	8
14-07-17	4.66	16-07-17 13.77h	2.38	22	14-07-17	1:25	-0.10	1200	H	S06W29	M2.4/--	2665		$\beta$	440	26
04-09-17	22.5	06-09-17 12.58h	1.59	210	04-09-17	20:12	47.50	1418	H	S10W12	M5.5/--	2673		$\beta\gamma$	130	12
06-09-17	12.58	09-09-17 19.11h	3.27	844	06-09-17	12:24	-0.30	1571	H	S08W33	X9.3/--	2673		$\beta\gamma\delta$	880	33
10-09-17	16.42	15-09-17 5.11h	4.53	1490	10-09-17	16:00	-232.00	3163	H	>W90b	X8.2/--	2673		$\beta\gamma\delta$	530	8

